Crystal structure of BtrK, a decarboxylase involved in the (*S*)-4-amino-2-hydroxybutyrate (AHBA) formation during butirosin biosynthesis

Laura A. Rivas Arenas[a], Fernanda C. R. de Paiva[a], Nicolas de Oliveira Rossini[a], YanYan Li[b], Jonathan Spencer[c], Peter Leadlay[d] and Marcio V. B. Dias[ae]*

[a]Department of Microbiology, Institute of Biomedical Sciences ICB III, University of São Paulo, Av. Prof. Lineu Prestes, 1374, São Paulo, São Paulo, 05508-000, Brazil

[b]Laboratory Molecules of Communication and Adaptation of Microorganisms (MCAM). UMR7245, CNRS-Muséum National d'Histoire Naturelle, Paris, France

[c]Department of Biochemistry, University of Cambridge, Cambridge, England

[d]Department of Chemistry, University of Cambridge, Cambridge, England

[e]Department of Chemistry, University of Warwick, Coventry, UK

Correspondence email: mvbdias@usp.br

Abstract Butirosin is an aminoglycoside that has an (*S*)-4-amino-2-hydroxybutyrate (AHBA) moiety capable of preventing the attack of several aminoglycoside modifying enzymes. The biosynthesis and the attachment of the AHBA to the 2-deoxystreptamine (2-DOS) involve seven enzymes that use glutamate as a precursor. BtrK is a pyridoxal-5-phosphate (PLP)-dependent enzyme and performs the decarboxylation of a glutamyl moiety tethered to the peptidyl carrier protein BtrI during the AHBA biosynthetic pathway. The structure of BtrK was solved at 1.4 Å resolution and indicated a conserved folding. The PLP is covalently linked through a Schiff base to Lys49 and performs intensive hydrogen bond interactions with active residues that are also conserved in other members of type IV PLP-dependent enzymes. Additionally, a docking simulation indicates the possible anchoring of a substrate fragment constituted of O-*S*-γ-Lglutamylpantetheine-4′-phosphate. The glutamyl moiety forms a number of hydrogen bonds with the putative active site residues of BtrK. The pantetheine moiety seems to perform only a few interactions and should adopt a more flexible conformation. The description of BtrK structure contributes to the understanding of the large family of PLP-dependent enzymes and also in this crucial step during the butirosin biosynthesis.

Keywords: aminoglycosides, butirosin, AHBA, (S)-4-amino-2-hydroxybutyrate, decarboxylase, PLP-dependent enzymes

Highlights:

- Structural characterization of BtrK, a decarboxylase involved in the biosynthesis of butirosin, was performed.
- BtrK has a structure similar to diaminopimelic acid decarboxylases (DAPDC), including the essential residues of the active site.

- The molecular docking of a truncated version of the substrate indicates a hypothetical binding mode of the glutamate tethered to the Peptidyl Carrier Protein (PCP) BtrI.

1. Introduction

Aminoglycosides are an important class of antibiotics that are used for the treatment of serious infections caused by Gram-negative (e.g., *Enterobacteriaceae*, *Acinetobacter*, *Pseudomonas*) and several Gram-positive bacteria [1–3], despite their nephrotoxic and ototoxic side effects [4–6]. Aminoglycoside mechanism of action involves interference with protein synthesis. These antibiotics bind to the 30S ribosome subunit causing errors in translation, specifically on codon reading, leading to protein mistranslation [2,3]. Aminoglycoside producers are predominantly from the *Actinomyces* bacteria group. These antibiotics are constituted by highly functionalized amino-sugars and deoxy-sugars linked by glycosidic bonds to an aminocyclitol aglycone [7]. Most aminoglycosides have a 2-deoxystreptamine (2-DOS) moiety as an aglycone, with different amino-sugars attached to the carbons 4 and 5 or 4 and 6 such as in kanamycin, gentamicin, and neomycin [8]. In recent years, there were great advances in the understanding of biosyntheses and in the enzymology of several biosynthetic steps from aminoglycosides, particularly those 2-DOS-containing molecules [9–16].

In contrast to most aminoglycosides, butirosin is so far the unique member of this class of antibiotics which is not produced by actinomyces but from *Bacillus circulans* [17]. Besides, butirosin has an unusual (*S*)-4-amino-2-hydroxybutyrate (AHBA) group attached to the C-1 amine of the 2-DOS moiety [18,19]. This peculiarity of butirosin is particularly interesting since the addition of AHBA to this position prevents the attack of several aminoglycoside modifying enzymes (AMEs), such as aminoglycoside *N*-acetyltransferases (AAC) [20], which lead to aminoglycoside resistance. The AHBA moiety of butirosin also further inspired the semisynthesis of the blockbuster aminoglycoside amikacin, which has an AHBA group attached to the C-1 of 2-DOS aglycone of kanamycin [21]. Among all available aminoglycosides, amikacin is one of the few that can overcome different AMEs mechanisms and, consequently, is one of the most used antibiotics from this class [22]. Hence, the understanding of the AHBA biosynthesis has strong relevance in the biotechnological process aiming to obtain new derivatives of aminoglycosides that overcome resistance mechanisms [23,24].

The biosynthesis of the AHBA group was elucidated in the butirosin biosynthetic gene cluster (BGC), and the functions of all involved enzymes were validated [25,26]. The seven genes responsible for producing this moiety (*btrI, btrK, btrG, btrH, btrO, btrJ,* and *btrV*) are exclusive to the butirosin gene cluster and its biosynthesis starts using L-glutamate as a precursor. This amino acid is further tethered to the peptidyl carrier protein (PCP) BtrI, which is successively decarboxylated, hydroxylated and transferred to the 2-DOS aglycone of ribostamycin to produce butirosin **(Fig. 1)**. The decarboxylation reaction is catalyzed by BtrK converting the precursor γ-L-glutamate-S-BtrI to γ-aminobutyric acid

(GABA)-*S*-BtrI. BtrK has also been proved to weakly decarboxylate free amino acids, including L-ornithine, L-arginine, L-lysine, and diaminopimelate (DAP) [25]. Based on the sequence, BtrK is a type IV pyridoxal-5-phosphate (PLP)-dependent decarboxylase that forms a Schiff-base with a conserved lysine of the protein's active site. Although the enzymes involved in the biosynthesis of AHBA have strong potential in synthetic biology, there is no structural analysis for any of them. Particularly for the BtrK, there is a structure deposited on PDB (2J66) but so far, at least to our knowledge, there is no description about it in the literature. Thus, to gain insights into the mechanism of the decarboxylation reaction during the biosynthesis of AHBA, we structurally characterized the *holo*-BtrK in complex with its coenzyme PLP at a higher resolution than that one previously deposited in PDB and performed a docking simulation to obtain insights into the possible binding mode of the L-glutamate by itself and forming an external aldimine with PLP (O-*S*-γ-L-glutamylpantetheine-4′-phosphate).

2. Methods

2.1. Protein Expression and Purification of Recombinant BtrK

Construction of the *btrK* expression plasmid was previously described [25]. The *btrK* gene coding region was amplified by PCR from genomic DNA of *Bacillus circulans* NR3312 and cloned into pET-28a(+) with six N-terminal His-tag. BL21(DE3) Rosetta cells were transformed with the expression plasmid and grown in LB media at 37°C until OD_{600nm} reached 0.6 with kanamycin selection (50 µg/mL). For protein overexpression, the cells were induced by the addition of isopropyl-β-D-1-thiogalactopyranoside (IPTG) at 0.2 mM and the growth was continued at 16°C overnight. Cells were harvested by centrifugation at 4186 *g* for 15 min at 4°C.

For purification, the cells were resuspended in 80 mL of binding buffer (20 mM Tris-HCl pH 7.9, 500 mM NaCl, 5 mM imidazole, 10% glycerol) with the addition of 0.1 mg/mL of DNAse, 1 mg/mL of lysozyme and 1 mM of phenylmethylsulfonyl fluoride (PMSF). Cells were disrupted by sonication and the solution was centrifuged at 39000 *g* for 1 hour to remove cell debris. His_6-tag BtrK was purified by His-tag affinity using a Ni^{2+}-NTA column. The elution was carried out in an HPLC Äkta system using a gradient with the elution buffer (20 mM Tris-HCl pH 7.9, 500 mM NaCl, 500 mM imidazole, 10% glycerol). BtrK was further purified by gel filtration using a Superdex 16/600 75 pg column (GE Healthcare Life Science). The fractions containing the protein were harvested and concentrated up to approximately 10 mg/mL. The protein was stored in a buffer consisting of 100 mM MOPS, and 5% glycerol at pH 7.0 for crystallization experiments.

2.2. Crystallization, Data Collection and Structure determination

Preliminary crystallization experiments were carried out using sitting-drop assays using 96 well plates containing different crystallization conditions (Hampton Research Corp.). Drops of 0.4 µL with a proportion of 1:1 of crystallization solution and protein solution at 10 mg/mL were prepared using an Oryx6 robot (Douglas Instruments Ltd.) and maintained at 20°C. After obtaining hits, crystals were optimized by hanging-drop experiments carried out manually using 24-well Linbro plates at 20°C. The best rectangular and square prismatic crystals were obtained in a condition constituted of 14% PEG 400, 100 mM MES pH 6.5 and 200 mM $MgCl_2$. For data collection, crystals were fished out using nylon loops (Hampton Research), cryoprotected in a condition composed of 30% ethylene glycol and 70% well solution and subsequently frozen using liquid nitrogen.

X-ray data collection was effected at DESy PETRA III Beamline P13, Germany and the X-ray data sets were processed using XDS [27] and scaled using AIMLESS [28] from CCP4i [29].

The structure of BtrK in complex with PLP was solved by molecular replacement using Phaser [30] from Phenix suite [31] and the PDB entry 2J66 [32] as a search model. The model refinement was performed using Phenix. Refine [31]. The inspection and manual construction of the models were carried out by Coot [33] using electronic density maps $2F_o$-F_c and F_o-F_c. The crystallographic analysis was performed by monitoring R_{factor} and R_{free} values and the stereochemistry quality of the final models was assessed by the MolProbity [34]. The final crystallographic structure was analyzed using Coot and the final figures were prepared using PyMOL (The PyMOL Molecular Graphics System, Schrödinger, LLC).

2.3. Molecular docking with alternative substrates

To evaluate the possible interaction between BtrK and the substrate, we performed docking simulations using the BtrK structure as a receptor and a short-truncated version of the external aldimine constituted of the L-glutamate tethered to the 4′-phosphopantetheine prosthetic group of the *holo*-BtrI and PLP as ligand. Alternatively, we also used L-glutamate by itself as a ligand. For this purpose, the ligands L-glutamate and the intermediate PLP-*O*-[*S*-γ-Lglutaylpantetheine-4′-phosphate]-serine were built and energy minimized using ChemDraw and ligand torsions were observed using the Autodock tools. Docking simulations were executed using AutoDock Vina Tools [35] and GOLD [36] and analyzed using PyMOL [37]. Standardization of the protonation state of the protein as built up with the automatic addition of hydrogens using the online server Protoss from Protein Plus (https://proteins.plus/help/protoss) [38]. Also, was performed a redocking, for which the PLP extracted from 7RU7 PDB entry, was used as ligand. The best obtained PLP poses were compared with the native PLP position bound to BtrK. The best parameters obtained in the redocking were defined including atoms up to 6Å distant from PLP's original position from PDB 2J66. The scoring function was selected as CHEMPLP and search efficiency as 100%. Once we have established that, docking simulations using

external-aldimine as the ligand and BtrK as the receptor were performed with the same redocking parameters.

For the docking using the program Autodock Vina, the receptor was prepared by the software Openbabel [39] for atom-typing and charge assignment using Gasteiger–Marsili charges [40]. The redocking of PLP was also used against BtrK using the default parameters. For the docking of L-glutamate grid, box characteristics were defined according to the PLP original position, which include a box of 18Å (x), 18Å (y) and 18Å (z); and the coordinates 2.495(x), 242.806(y) and -35.27(z).

3. Results and discussion

3.1. The overall structure of BtrK

Crystals for BtrK in complex with PLP have diffracted up to 1.4 Å resolution and they belong to the space group $P2_12_12$. The structure of BtrK-PLP was solved by molecular replacement and the refined structure had a final R_{work} of 17.8% and R_{free} of 19.5%. The final model has 3648 non-hydrogen atoms and the region between the residues 312 to 317 was not modeled because of the absence or weak electron density indicating high flexibility. Further crystallographic and refinement statistics of BtrK-PLP are summarized in **Tables 1 and 2**. Attempts to obtain the structure in complex with the alternative substrates L-arginine and L-ornithine were performed, but we did not observe the corresponding electron density in the active site. Li *et al*. (2005) reported that the activity of BtrK over free amino acids is very low and consequently their affinity should be weak, suggesting that the glutamate tethered to the BtrI should play an important role in BtrK catalysis.

The overall folding of BtrK confirms that this enzyme belongs to the type IV PLP-dependent decarboxylases and has an N-terminal domain consisting of an 8-fold α/β-barrel and a C-terminal β-sandwich Greek key motif domain **(Fig. 2**A**)**. The α/β-barrel opens with an α-helix instead of a β-strand such as classic TIM barrels. In proteins with this folding, PLP is located in the C-terminal of the α/β-barrel, at the domain interface. Despite the asymmetric unit of BtrK crystal having a single protomer, a homodimer with a head-to-tail arrangement can also be obtained using symmetry operations. In this arrangement, the α/β-barrel of one monomer interacts with the β-sandwich domain of the adjacent protein molecule **(Fig. 2**B**).** The homodimer quaternary structure was also confirmed by analytical gel filtration analysis (data not shown). The dimerization surface interaction has an area of about 3450Å according to the web server PDBePISa [41] indicating a tight interaction between the subunits. The dimer is predominantly stabilized by hydrophobic interactions between the two subunits, although there are also some hydrogen interactions (31 in total) and 4 ionic interactions, according to PDBSum [42].

Analysis of the electrostatic potential surface of the BtrK monomer indicates the coexistence of positive and negative charges, but the active site pocket has a predominance of electropositive charges in the most exposed regions and negative charges in the most buried ones **(Fig. S1**A**)**. Additionally, according

to the hydrophobicity model of the protein using YRB (yellow, red, blue) system [43], the center of the β-sheet of the α/β-barrel is predominantly hydrophobic **(Fig. S1**B**)**, as expected, and that should be crucial for the protein oligomerization.

3.2. Structure and sequence comparison to other type IV-PLP dependent enzymes

A search performed on the DALI database returned several diaminopimelic acid decarboxylases (DAPDC) as the most similar structures, sharing about 30-20% of amino acid sequence similarities. These enzymes belong to the type IV PLP-dependent decarboxylase family, and they share a r.m.s.d. for all atoms based on the DALI database of about 1.2 to 1.4 Å. The superposition of BtrK (PDB code 7ru7) with other DAPDC including the *Helicobacter pylori* DAPDC (*Hp*DAPDC; PDB code 2qgh) [44], *Aquifex aeolicus* DAPDC (*Aa*DAPDC; PDB code 2p3e) (data not published), *Methanococcus jannaschii* DAPDC (*Mj*DAPDC; PDB code 1twi) [45], and *Staphylococcus aureus* DAPDC (*Sa*DAPDC; PDB code 6kni) [46] indicates that the overall folding is conserved **(Fig. 3**A**)**. The most prominent differences are observed in the active site loop **(Fig. 3**B**)**. As described previously for other members of the DAPDC family, the active site loop is the most diverse region among these enzymes [44].

In BtrK, the active site loop creates a ceiling for the active site and should act as a lid on the substrate binding. It could have a key function in the anchoring of BtrI-glutamate substrate in the active site cavity. Different from the other DAPDCs, BtrK active site loop (Asn140-Asp162) adopts an opener conformation that should reflect the absence of the substrate binding pocket **(Fig. S2**A,B**)**. This hypothesis is based on the superposition of these regions and on what was reported for the *Hp*DAPDC, whose active site loop is in an engaged conformation that protects the ligand from the solvent bulk **(Fig. S2**A,C**)** [44]. Besides, this loop could oscillate from an open to a closed conformation according to the absence or presence of the substrate, respectively. The loops from the *Hp*DAPDC and *Mj*DAPDC also form an α-helix that might contribute to the active site architecture formation and stability **(Fig. 3**B and **Fig. S2**C,D**)**. On the other hand, in the absence of substrate, the active site loop can also be highly flexible as observed for *Aa*DAPDC and *Sa*DAPDC, whose regions were not modeled because of the absence of electron density **(Fig. S2**E,F**).**

Furthermore, the "specificity element", generally described as a 3_{10}-helix, located at the back of the active site pocket [46], might also differ among different decarboxylases **(Fig. 3**C**)**. In BtrK, this region was not fully modeled because of the absence of electron density. Still, we assume that it may adopt the same conformation as the other specificity elements from the DAPDC protein family, which means a regular α-helix. Due to the proximity of the specificity element to the PLP, different decarboxylases can act on substrates of various sizes and their amino acid sequences should determine the specificity of the interaction [47].

A BLAST search using the amino acid sequence of BtrK was also performed and the most similar sequences are type IV PLP-dependent decarboxylases with unknown functions or putative diaminopimelic decarboxylases from several *Bacillus* species. However, although most of the sequences cover the full length of BtrK, the identity is only about 50-40%, suggesting that this enzyme should be quite specialized for its function in the AHBA biosynthesis and the anchoring of BtrI. A sequence alignment of BtrK with the other DAPDC was performed using ESPript 3.0 (https://espript.ibcp.fr) [48], which indicates that a number of sequential motifs are conserved **(Fig. S3)**. These include the KAN motif, in which the lysine residue performs a covalent interaction with the PLP; the glycine-rich region GGG which is involved in the interaction with the phosphate moiety of PLP and the GAYG motif. Interestingly, BtrK does not conserve the classic HIGS motif, which participates in the protonation and deprotonation reactions [49]. The histidine and serine from this motif are substituted to tyrosine and threonine, respectively. The EPGR motif also has a substitution in BtrK, in which the proline is replaced by a serine.

Using the ConSurf server [50], it was possible to identify the conserved residues based on phylogenetic evolution between the homolog sequences. The α/β-barrel has a high conserved structure, particularly in the C-terminal region, where PLP is anchored **(Fig. S4)**. In contrast, the α-helices are more flexible and it is expected that their amino acids are highly variable. The positions of the catalytic residues are also conserved throughout evolution for optimal access to the substrate. The β-sandwich domain is also partially conserved, in which residues from the β-sheets of this motif seem to be highly similar in contrast to the residues from the α-helices that are much less conserved **(Fig. S4)**.

3.3. The PLP binding site

The BtrK active site is located in a deep and large groove between the two protomers that form the homodimer, which is consistent with the anchoring of the BtrI-substrate. PLP is covalently bound to the conserved Lys49 via Schiff base forming an internal aldimine according to the electron density tracing **(Fig. 4**A,B**)**. The PLP phosphate group forms hydrogen bonds with Tyr187 (2.8 Å), Thr190 (2.6 Å), Gly271 (2.9 Å), Arg272 (2.8 Å), and Tyr375 (2.6 Å) **(Fig. 4**A and **Fig. S5)**. In addition, the PLP phosphate group also interacts *via* water molecules with other conserved amino acid residues, particularly Glu269, Arg272, and Gly228. The PLP pyridine nitrogen interacts with the conserved Glu269 through ionic bonds. This interaction could contribute to maintaining the positive charge on the pyridine nitrogen and consequently, increment the electron-withdrawing capacity of the ring, as reported for ornithine decarboxylases (ODC) [51,52], histidine decarboxylase (HDC) [53] or even other L-amino acid decarboxylases (AADCs) [54–56]. Although PLP is near to the interface of both protomers, each one of the PLPs from the dimer has a predominance of hydrogen interactions with residues of a single subunit protomer. However, Cys346 from the adjacent protomer is a nearby residue that should play a role in the catalytic mechanism of the enzyme **(Fig. 4**A**)**. Cys346 is conserved among

several decarboxylases and should be involved in the correct protonation of the Cα from the intermediate during the decarboxylation reaction [57]. Although the sulphydryl side-chain of Cys346 is positioned away from the hypothetical substrate binding site and also from PLP, in other decarboxylases, including eukaryotic decarboxylases and the AADC SbnH from *S. aureus* (*Sa*DAPDC*)*, this cysteine should rotate to correct perform its role during the decarboxylation reaction [46,57,58].

The analysis of the electrostatic potential of the active site indicated that the PLP phosphate group is located in a slightly negative charge region while the pyrimidine moiety of PLP is surrounded by a predominance of positive charges **(Fig. 4**C**).**

The PLP pyridine ring performs a π-π stacking interaction at the *si*-face with the hydroxyphenyl side chain of Tyr187 **(Fig. 4**B**)** rather than with a histidine which is a very well conserved residue of HIGS motif from other DAPDCs **(Fig. 5)** [49]. This conserved histidine has an important role in the decarboxylation process since it stabilizes the PLP and helps to orientate the Cα-C ligation near the π-system to be subsequently cleaved [59]. Generally, phenylalanine, tyrosine and tryptophan residues have stronger interactions with 6-membered rings while histidine performs a more stable interaction with 5-membered rings [60]. Consequently, this amino acid substitution could help the PLP to anchor at the BtrK active site on a more stable interaction than those in other similar decarboxylases.

3.4. Substrate binding site and binding mode

In order to predict the binding mode of the BtrK substrate in the active site, we have performed a molecular docking simulation using the hypothetical external aldimine of BtrK intermediate, PLP-*O*-[*S*-γ-Lglutaylpantetheine-4′-phosphate]serine (a long truncated version of the substrate, in which the glutamate is tethered to the coenzyme A and covalently linked to PLP) **(Fig. 6**A**)**.

According to the electrostatic potential, the active site should be more favorable to the binding of substrates with negative charges as L-glutamate and the *holo*-BtrI prosthetic arm should be more exposed and located in a cavity with mainly positive and neutral charges **(Fig. S6)**.

The PLP moiety of the docked external aldimine is in a similar position to that from the BtrK crystal structure, without affecting the π-stacking interaction distance with Tyr187 **(Fig. 6**B**)**. The PLP phosphate group is interacting through hydrogen bonds with Gly271, Arg272, Tyr375 and Thr190 **(Fig. 6**B). Thr190 might also contribute to stabilizing the substrate through the interaction with the δ-carboxyl group of L-glutamate, as well as Tyr375 and Tyr187. The substrate is also interacting with Arg157, specifically with the phosphopantetheine and Ser41 that is part of BtrI. The docking score for PLP-*O*-[*S*-γ-Lglutaylpantetheine-4′-phosphate]serine was 64.3704. To increase our confidence, a PLP redocking was carried out using GOLD and Vina programs and we observed a good r.m.s.d. between the experimental and docked positions **(Fig. S7)**. The score functions for the redocked PLP were -6.4 kcal/mol and 46.963 for Vina and GOLD, respectively.

Another reference of our docking simulation was the comparison with the *Sa*DAPDC substrate, citryl-diaminoethane (citryl-Dae) **(Fig. 6**C**)**, considering that they bind in a similar position. The pyridine rings from PLP are almost aligned to each other and the phosphate groups perform conserved interactions with glycine residues (Gly271 and Gly268) from the EPGR conserved motif. The L-isomer substrate of *Sa*DAPDC and the phenolic oxygen of the PLP pyridine ring interacts with the key active site Cys344 from the adjacent protomer [46], while for BtrK, we did not observe such interaction. There are other conserved residues near the active site, including Arg269, which interact with the carboxyl group of citryl-Dae in the *Sa*DAPDC. Instead, the carboxyl group of L-glutamate (external aldimine) interacts with Tyr375 in BtrK. Likewise, we carried out the docking of the L-glutamate by itself **(Fig. 6D)** and we observed an interaction with Cys346 of the adjacent protomer that should be involved in the stabilization of the substrate by the α-amino group of L-glutamate and consequently would contribute to its decarboxylation. The α-carboxyl group of L-glutamate makes contacts with Arg157, and the δ-carboxyl group conserved the bond with Thr190 and Arg272. The score of the L-glutamate docking was -4.0 kcal/mol.

Based on the conservation of active site residues and prediction of the binding mode of the substrate, BtrK should have a similar catalytic mechanism to other DAPDCs, in which Cys346 from the adjacent subunit could play a key role in the Schiff base formation, carbonation protonation and finally the decarboxylation reaction. The other residues of the active site should contribute to modulating the positive and negative charges for catalysis, correct positioning of the substrate and stabilizing the external and the resting state of internal aldimine.

4. Conclusion

In summary, we described the structure of the *holo*-BtrK, a key decarboxylase involved in the biosynthesis of AHBA moiety of the aminoglycoside butirosin. BtrK has a similar structure to other type IV decarboxylases as DAPDC and ODC, despite its modest sequence similarity to other solved structures. The most prominent difference includes several regions of loops, especially the active site loop that might be involved in specialization for the anchoring of the substrate tethered to the BtrI. Interestingly, the HIGS motif is not fully conserved in BtrK. Instead of a histidine, there is a tyrosine that forms a π-π system and also the serine of this motif is substituted by threonine which should contribute to stabilizing the PLP in the active site. In addition, the comparison between BtrK and other DAPDCs indicates that it was obtained in an open conformation state that should reflect the absence of the substrate in the active site. The active site of BtrK is located in the interface of the two subunits and conserves most of the residues in comparison with other type IV decarboxylases. Based on the binding mode of PLP and in a docking simulation using L-glutamate and the hypothetical external aldimine

PLP-*O*-[*S*-γ-Lglutaylpantetheine-4′-phosphate]serine as ligand, we observed that the mechanism of catalysis of BtrK should be similar to other DAPDC or ODC, which involves a conserved cysteine residue that acts as a general basis. To our knowledge, this is the first structural description for an enzyme involved in the biosynthesis of AHBA from the butirosin biosynthesis. A better understanding of the butirosin biosynthesis might create opportunities for biosynthetic manipulation to produce new derivatives of aminoglycosides.

Funding sources

This project was founded by Conselho Nacional de Desenvolvimento Científico e Tecnológico CNPq (No. 133838/2018-8) and Fundação de Amparo à Pesquisa do Estado de São Paulo, (FAPESP) (process 2018/00351-1)

Declaration of competing interest

The authors declare no competing financial interests.

CRediT authorship contribution statement

M.V.B.D. (Marcio V.B. Dias) conceived and led the project; J.S. (Jonathan Spencer) and P.L. (Peter Leadlay) conceived the project and supervised the cloning of btrK; YY.L. (YanYan Li) performed the cloning of *btrK* from *B. circulans*; L.A.R.A. (Laura A. Rivas Arenas) performed the protein production, purification, crystallization; L.A.R.A and F.R.D.P (Fernanda Rodrigues de Paiva) performed the structure determination and analysis; N.O.R. (Nicolas de Oliveira Rossini) performed the docking simulations and analysis; LARA and MVBD wrote the manuscript and all authors read, corrected and approved the manuscript.

Acknowledgements

We would like to thank Dr. Fanglu Huang from the University of Cambridge, the UK for fruitful discussions and reading our manuscript and Dr. Isabel Bento from EMBL c/o Desy, Germany for the assistance in X-ray data collection.

References

[1] K.M. Krause, A.W. Serio, T.R. Kane, L.E. Connolly, Aminoglycosides : An Overview, (2016) 1–18. https://doi.org/10.1101/cshperspect.a027029.

[2] R.S. Edson, C.L. Terrell, The Aminoglycosides, Mayo Clin. Proc. 74 (1999) 519–528. https://doi.org/10.4065/74.5.519.

[3] L.P. Kotra, J. Haddad, S. Mobashery, Aminoglycosides: Perspectives on mechanisms of action and resistance and strategies to counter resistance, Antimicrob. Agents Chemother. 44 (2000) 3249–3256. https://doi.org/10.1128/AAC.44.12.3249-3256.2000.

[4] Y. Takahashi, M. Igarashi, Destination of aminoglycoside antibiotics in the "post-antibiotic era," J. Antibiot. (Tokyo). 71 (2018) 4–14. https://doi.org/10.1038/ja.2017.117.

[5] D.P. Arya, Aminoglycoside Antibiotics: From Chemical Biology to Drug Discovery, John Wiley & Sons, Inc., New Jersey, 2007.

[6] F. Kudo, T. Eguchi, Aminoglycoside Antibiotics : New Insights into the Biosynthetic Machinery of Old Drugs, (2016) 4–18. https://doi.org/10.1002/tcr.201500210.

[7] F. Kudo, T. Eguchi, Biosynthetic genes for aminoglycoside antibiotics, J. Antibiot. (Tokyo). 62 (2009) 471–481. https://doi.org/10.1038/ja.2009.76.

[8] F. Kudo, T. Eguchi, Chapter 20: Biosynthetic Enzymes for the Aminoglycosides Butirosin and Neomycin, 1st ed., Elsevier Inc., 2009. https://doi.org/10.1016/S0076-6879(09)04620-5.

[9] N.C. De Araújo, P.D.S. Bury, M.T. Tavares, F. Huang, R. Parise-Filho, P. Leadlay, M.V.B. Dias, Crystal Structure of GenD2, a NAD-Dependent Oxidoreductase Involved in the Biosynthesis of Gentamicin, ACS Chem. Biol. 14 (2019) 925–933. https://doi.org/10.1021/acschembio.9b00115.

[10] P.D.S. Bury, F. Huang, S. Li, Y. Sun, P.F. Leadlay, M.V.B. Dias, Structural Basis of the Selectivity of GenN, an Aminoglycoside N-methyltransferase Involved in Gentamicin Biosynthesis, ACS Chem. Biol. 12 (2017) 2779–2787. https://doi.org/10.1021/acschembio.7b00466.

[11] F. Kudo, Y. Kitayama, A. Miyanaga, M. Numakura, T. Eguchi, Stepwise Post-glycosylation Modification of Sugar Moieties in Kanamycin Biosynthesis, ChemBioChem. 22 (2021) 1668–1675. https://doi.org/10.1002/cbic.202000839.

[12] R. Takeishi, F. Kudo, M. Numakura, T. Eguchi, Epimerization at C-3″ in butirosin biosynthesis by an NAD+-dependent dehydrogenase BtrE and an NADPH-dependent reductase BtrF, ChemBioChem. 16 (2015) 487–495. https://doi.org/10.1002/cbic.201402612.

[13] F. Kudo, T. Tokumitsu, T. Eguchi, Substrate specificity of radical S-adenosyl-l-methionine dehydratase AprD4 and its partner reductase AprD3 in the C3′-deoxygenation of aminoglycoside antibiotics, J. Antibiot. (Tokyo). 70 (2017) 423–428. https://doi.org/10.1038/ja.2016.110.

[14] T.R. Zachman-Brockmeyer, J.B. Thoden, H.M. Holden, The structure of RbmB from Streptomyces ribosidificus, an aminotransferase involved in the biosynthesis of ribostamycin, Protein Sci. 26 (2017)

1886–1892. https://doi.org/10.1002/pro.3221.

[15] Y.H. Ban, M.C. Song, J. yeon Hwang, H. lyung Shin, H.J. Kim, S.K. Hong, N.J. Lee, J.W. Park, S.S. Cha, H. wen Liu, Y.J. Yoon, Complete reconstitution of the diverse pathways of gentamicin B biosynthesis, Nat. Chem. Biol. 15 (2019) 295–303. https://doi.org/10.1038/s41589-018-0203-4.

[16] J. Zhang, X. Hou, Z. Chen, Y. Ko, M.W. Ruszczycky, Y. Chen, J. Zhou, H.-W. Liu, Dioxane Bridge Formation during the Biosynthesis of Spectinomycin Involves a Twitch Radical S-Adenosyl Methionine Dehydrogenase That May Have Evolved from an Epimerase., J. Am. Chem. Soc. (2022). https://doi.org/10.1021/jacs.2c02676.

[17] J.D. Howells, L.E. Anderson, G.L. Coffey, G.D. Senos, M.A. Underhill, D.L. Vogler, J. Ehrlich, Butirosin, a new aminoglycosidic antibiotic complex: bacterial origin and some microbiological studies., Antimicrob. Agents Chemother. 2 (1972) 79–83. https://doi.org/10.1128/AAC.2.2.79.

[18] H. Dion, P. Woo, N. Willmer, D. Kern, J. ONAGA, S. FUSARI, Butirosin, a new aminoglycosidic antibiotic complex: isolation and characterization, Antimicrob. Agents Chemother. 2 (1972) 84–88. http://aac.asm.org/content/2/2/84.short.

[19] F. Kudo, M. Numakura, H. Tamegai, H. Yamamoto, T. Eguchi, K. Kakinuma, Extended sequence and functional analysis of the butirosin biosynthetic gene cluster in Bacillus circulans SANK 72073, J. Antibiot. (Tokyo). 58 (2005) 373–379. https://doi.org/10.1038/ja.2005.47.

[20] K.J. Labby, S. Garneau-Tsodikova, Strategies to overcome the action of aminoglycoside-modifying enzymes for treating resistant bacterial infections, Future Med. Chem. 5 (2013) 1285–1309. https://doi.org/10.4155/fmc.13.80.

[21] S.G. Zárate, M.L. De La Cruz Claure, R. Benito-Arenas, J. Revuelta, A.G. Santana, A. Bastida, Overcoming aminoglycoside enzymatic resistance: Design of novel antibiotics and inhibitors, Molecules. 23 (2018). https://doi.org/10.3390/molecules23020284.

[22] M.S. Ramirez, M.E. Tolmasky, Amikacin: Uses, resistance, and prospects for inhibition, Molecules. 22 (2017). https://doi.org/10.3390/molecules22122267.

[23] N.M. Llewellyn, J.B. Spencer, Biosynthesis of 2-deoxystreptamine-containing aminoglycoside antibiotics, Nat. Prod. Rep. 23 (2006) 864–874. https://doi.org/10.1039/b604709m.

[24] N.M. Llewellyn, J.B. Spencer, Chemoenzymatic acylation of aminoglycoside antibiotics, Chem. Commun. (2008) 3786–3788. https://doi.org/10.1039/b802248h.

[25] Y. Li, N.M. Llewellyn, R. Giri, F. Huang, J.B. Spencer, Biosynthesis of the unique amino acid side chain of butirosin: Possible protective-group chemistry in an acyl carrier protein-mediated pathway, Chem. Biol. 12 (2005) 665–675. https://doi.org/10.1016/j.chembiol.2005.04.010.

[26] N.M. Llewellyn, Y. Li, J.B. Spencer, Biosynthesis of Butirosin: Transfer and Deprotection of the Unique Amino Acid Side Chain, Chem. Biol. Cell Press. 14 (2007) 379–386. https://doi.org/10.1016/j.chembiol.2007.02.005.

[27] W. Kabsch, XDS, Acta Crystallogr D Biol Crystallogr. 66 (2010) 125–132. https://doi.org/10.1107/S0907444909047337.

[28] P. Evans, Scaling and assessment of data quality, Acta Crystallogr D Biol Crystallogr. 62 (2006) 72–82. https://doi.org/10.1107/S0907444905036693.

[29] M.D. Winn, C.C. Ballard, K.D. Cowtan, E.J. Dodson, P. Emsley, P.R. Evans, R.M. Keegan, E.B. Krissinel, A.G. Leslie, A. McCoy, S.J. McNicholas, G.N. Murshudov, N.S. Pannu, E.A. Potterton, H.R. Powell, R.J. Read, A. Vagin, K.S. Wilson, Overview of the CCP4 suite and current developments, Acta Crystallogr D Biol Crystallogr. 67 (2011) 235–242. https://doi.org/10.1107/S0907444910045749.

[30] A.J. McCoy, R.W. Grosse-Kunstleve, P.D. Adams, M.D. Winn, L.C. Storoni, R.J. Read, Phaser crystallographic software, J Appl Crystallogr. 40 (2007) 658–674. https://doi.org/10.1107/S0021889807021206.

[31] P. V Afonine, R.W. Grosse-Kunstleve, N. Echols, J.J. Headd, N.W. Moriarty, M. Mustyakimov, T.C. Terwilliger, A. Urzhumtsev, P.H. Zwart, P.D. Adams, Towards automated crystallographic structure refinement with Phenix. refine, Acta Crystallogr D Biol Crystallogr. 68 (2012) 352–367. https://doi.org/10.1107/S0907444912001308.

[32] B. Popovic, Y. Li, D.Y. Chirgadze, T.L. Blundell, J.B. Spencer, Structural Characterisation of BtrK Decarboxylase from Bacillus circulans Butirosin Biosynthesis, (2006). https://doi.org/10.2210/pdb2J66/pdb.

[33] P. Emsley, K. Cowtan, Coot: model-building tools for molecular graphics, Acta Crystallogr D Biol Crystallogr. 60 (2004) 2126–2132. https://doi.org/10.1107/S0907444904019158.

[34] V.B. Chen, W.B. Arendall, J.J. Headd, D.A. Keedy, R.M. Immormino, G.J. Kapral, L.W. Murray, J.S. Richardson, D.C. Richardson, MolProbity: all-atom structure validation for macromolecular crystallography, Acta Crystallogr D Biol Crystallogr. 66 (2010) 12–21. https://doi.org/10.1107/S0907444909042073.

[35] D.S. Goodsell, A.J. Olson, Automated docking of substrates to proteins by simulated annealing, Proteins Struct. Funct. Bioinforma. 8 (1990) 195–202. https://doi.org/10.1002/prot.340080302.

[36] G. Jones, P. Willett, R.C. Glen, A.R. Leach, R. Taylor, Development and validation of a genetic algorithm for flexible docking, J. Mol. Biol. 267 (1997) 727–748. https://doi.org/10.1006/jmbi.1996.0897.

[37] D. Seeliger, B.L. De Groot, Ligand docking and binding site analysis with PyMOL and Autodock/Vina,

J. Comput. Aided. Mol. Des. 24 (2010) 417–422. https://doi.org/10.1007/s10822-010-9352-6.

[38] S. Bietz, S. Urbaczek, B. Schulz, M. Rarey, Protoss: A holistic approach to predict tautomers and protonation states in protein-ligand complexes, J. Cheminform. 6 (2014). https://doi.org/10.1186/1758-2946-6-12.

[39] N.M. O'Boyle, C. Morley, G.R. Hutchison, Pybel: A Python wrapper for the OpenBabel cheminformatics toolkit, Chem. Cent. J. 2 (2008). https://doi.org/10.1186/1752-153X-2-5.

[40] J. Gasteiger, M. Marsili, Iterative partial equalization of orbital electronegativity-a rapid access to atomic charges, Tetrahedron. 36 (1980) 3219–3228. https://doi.org/10.1016/0040-4020(80)80168-2.

[41] E. Krissinel, K. Henrick, Inference of Macromolecular Assemblies from Crystalline State, J. Mol. Biol. 372 (2007) 774–797. https://doi.org/10.1016/j.jmb.2007.05.022.

[42] R.A. Laskowski, J. Jabłońska, L. Pravda, R.S. Vařeková, J.M. Thornton, PDBsum: Structural summaries of PDB entries, Protein Sci. 27 (2018) 129–134. https://doi.org/10.1002/pro.3289.

[43] D. Hagemans, I.A.E.M. van Belzen, T. Morán Luengo, S.G.D. Rüdiger, A script to highlight hydrophobicity and charge on protein surfaces, Front. Mol. Biosci. 2 (2015). https://doi.org/10.3389/fmolb.2015.00056.

[44] T. Hu, D. Wu, J. Chen, J. Ding, H. Jiang, X. Shen, The catalytic intermediate stabilized by a "down" active site loop for diaminopimelate decarboxylase from Helicobacter pylori: Enzymatic characterization with crystal structure analysis, J. Biol. Chem. 283 (2008) 21284–21293. https://doi.org/10.1074/jbc.M801823200.

[45] S.S. Ray, J.B. Bonanno, K.R. Rajashankar, M.G. Pinho, G. He, H. De Lencastre, A. Tomasz, S.K. Burley, Cocrystal Structures of Diaminopimelate Decarboxylase, Structure. 10 (2003) 1499–1508. https://doi.org/10.1016/s0969-2126(02)00880-8.

[46] J. Tang, Y. Ju, Q. Gu, J. Xu, H. Zhou, Structural Insights into Substrate Recognition and Activity Regulation of the Key Decarboxylase SbnH in Staphyloferrin B Biosynthesis, J. Mol. Biol. 431 (2019) 4868–4881. https://doi.org/10.1016/j.jmb.2019.10.009.

[47] J. Lee, A.J. Michael, D. Martynowski, E.J. Goldsmith, M.A. Phillips, Phylogenetic diversity and the structural basis of substrate specificity in the β/α-barrel fold basic amino acid decarboxylases, J. Biol. Chem. 282 (2007) 27115–27125. https://doi.org/10.1074/jbc.M704066200.

[48] X. Robert, P. Gouet, Deciphering key features in protein structures with the new ENDscript server, Nucleic Acids Res. 42 (2014) 320–324. https://doi.org/10.1093/nar/gku316.

[49] K. Gokulan, B. Rupp, M.S. Pavelka, W.R. Jacobs, J.C. Sacchettini, Crystal structure of Mycobacterium tuberculosis diaminopimelate decarboxylase, an essential enzyme in bacterial lysine biosynthesis, J.

Biol. Chem. 278 (2003) 18588–18596. https://doi.org/10.1074/jbc.M301549200.

[50] O. Goldenberg, E. Erez, G. Nimrod, N. Ben-Tal, The ConSurf-DB: pre-calculated evolutionary conservation profiles of protein structures, Nucleic Acids Res. 37 (2009) 323–327. https://doi.org/10.1093/nar/gkn822.

[51] N. V. Grishin, A.L. Osterman, H.B. Brooks, M.A. Phillips, E.J. Goldsmith, X-ray structure of ornithine decarboxylase from Trypanosoma brucei: The native structure and the structure in complex with α difluoromethylornithine, Biochemistry. 38 (1999) 15174–15184. https://doi.org/10.1021/bi9915115.

[52] A.L. Osterman, L.N. Kinch, N. V. Grishin, M.A. Phillips, Acidic Residues Important for Substrate Binding and Cofactor Reactivity in Eukaryotic Ornithine Decarboxylase Identified by Alanine Scanning Mutagenesis, J. Biol. Chem. 270 (1995) 11797–11802. https://doi.org/10.1074/jbc.270.20.11797.

[53] H. Komori, Y. Nitta, H. Ueno, Y. Higuchi, Structural study reveals that Ser-354 determines substrate specificity on human histidine decarboxylase, J. Biol. Chem. 287 (2012) 29175–29183. https://doi.org/10.1074/jbc.M112.381897.

[54] A. Okawa, T. Shiba, M. Hayashi, Y. Onoue, M. Murota, D. Sato, J. Inagaki, T. Tamura, S. Harada, K. Inagaki, Structural basis for substrate specificity of l-methionine decarboxylase, Protein Sci. 30 (2021) 663–677. https://doi.org/10.1002/pro.4027.

[55] A. Poupon, F. Jebai, G. Labesse, F. Gros, J. Thibault, J.P. Mornon, M. Krieger, Structure modelling and site-directed mutagenesis of the rat aromatic L- amino acid pyridoxal 5'-phosphate-dependent decarboxylase: A functional study, Proteins Struct. Funct. Genet. 37 (1999) 191–203. https://doi.org/10.1002/(SICI)1097-0134(19991101)37:2<191::AID-PROT5>3.0.CO;2-4.

[56] Q. Han, H. Ding, H. Robinson, B.M. Christensen, J. Li, Crystal structure and substrate specificity of Drosophila 3,4-dihydroxyphenylalanine decarboxylase, PLoS One. 5 (2010). https://doi.org/10.1371/journal.pone.0008826.

[57] L.K. Jackson, H.B. Brooks, A.L. Osterman, E.J. Goldsmith, M.A. Phillips, Altering the reaction specificity of eukaryotic ornithine decarboxylase, Biochemistry. 39 (2000) 11247–11257. https://doi.org/10.1021/bi001209s.

[58] R. Poulin, L. Lu, B. Ackermann, P. Bey, A.E. Pegg, Mechanism of the irreversible inactivation of mouse ornithine decarboxylase by α-difluoromethylornithine. Characterization of sequences at the inhibitor and coenzyme binding sites, J. Biol. Chem. 267 (1992) 150–158. https://doi.org/10.1016/s0021-9258(18)48472-4.

[59] J. Ni, G. Xu, W. Dai, Y.L. Zhao, Y. Ni, Hyperconjugation promoted by hydrogen bonding between His98/His241 and a carboxyl group contributes to tyrosine decarboxylase catalysis, Catal. Sci. Technol. 9 (2019) 6222–6226. https://doi.org/10.1039/c9cy01290g.

[60] M. Brylinski, Aromatic interactions at the ligand-protein interface: Implications for the development of docking scoring functions, Chem. Biol. Drug Des. 91 (2018) 380–390. https://doi.org/10.1111/cbdd.13084.Aromatic.

Figures

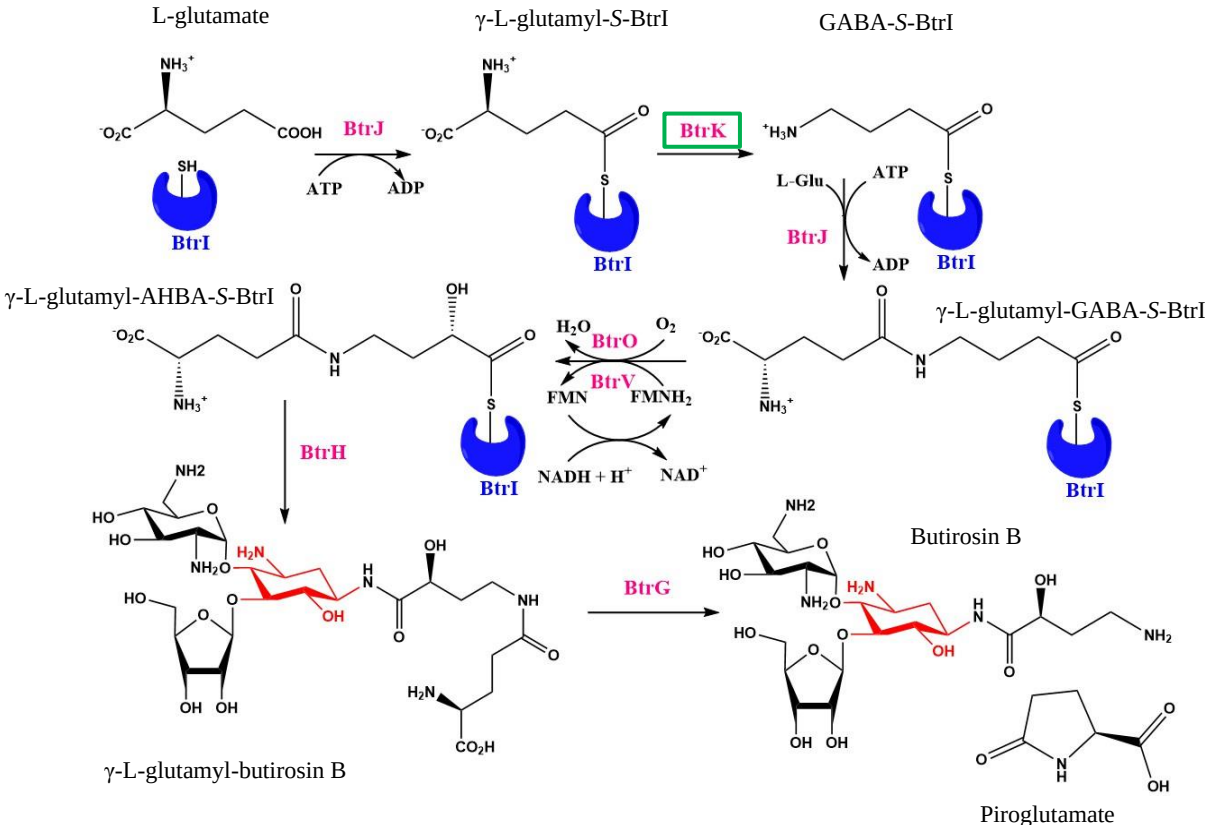

Fig 1. Biosynthesis of AHBA in butirosin B. The respective enzymes at each step are in pink and the PCP (BtrI) is in blue. The 2-DOS ring is shown in red.

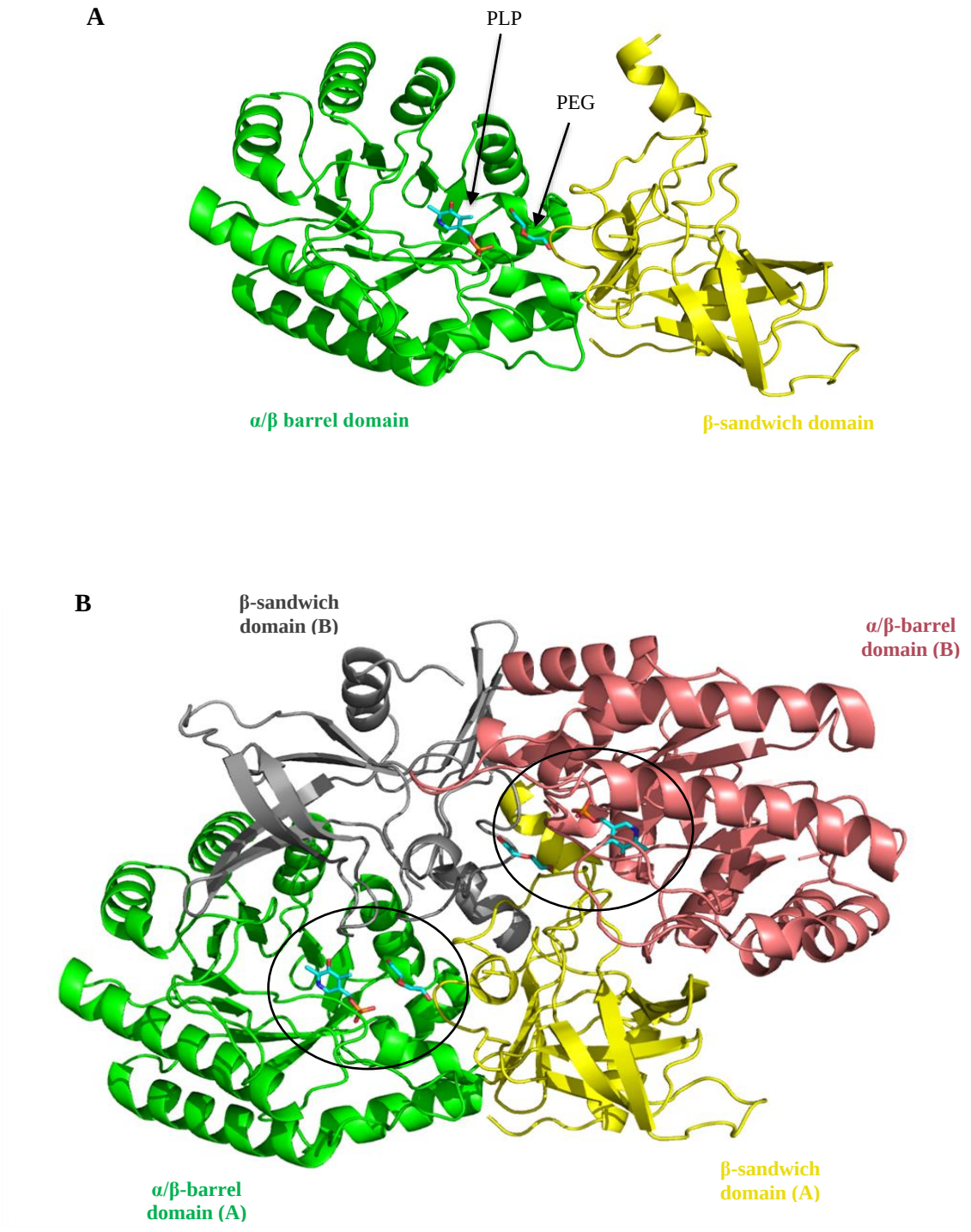

Fig. 2. The overall structure of BtrK decarboxylase. (A) BtrK monomer cartoon diagram with the N-terminal domain in green and C-terminal in yellow. PLP cofactor and PEG are represented in sticks distinguished by colors according to the atom (N, blue; C, cyan; O, red; P, orange). (B) BtrK homodimer cartoon diagram with the different N and C-domains identified by colors according to the chain (chains A and B). The circles indicate the two active sites of the enzyme.

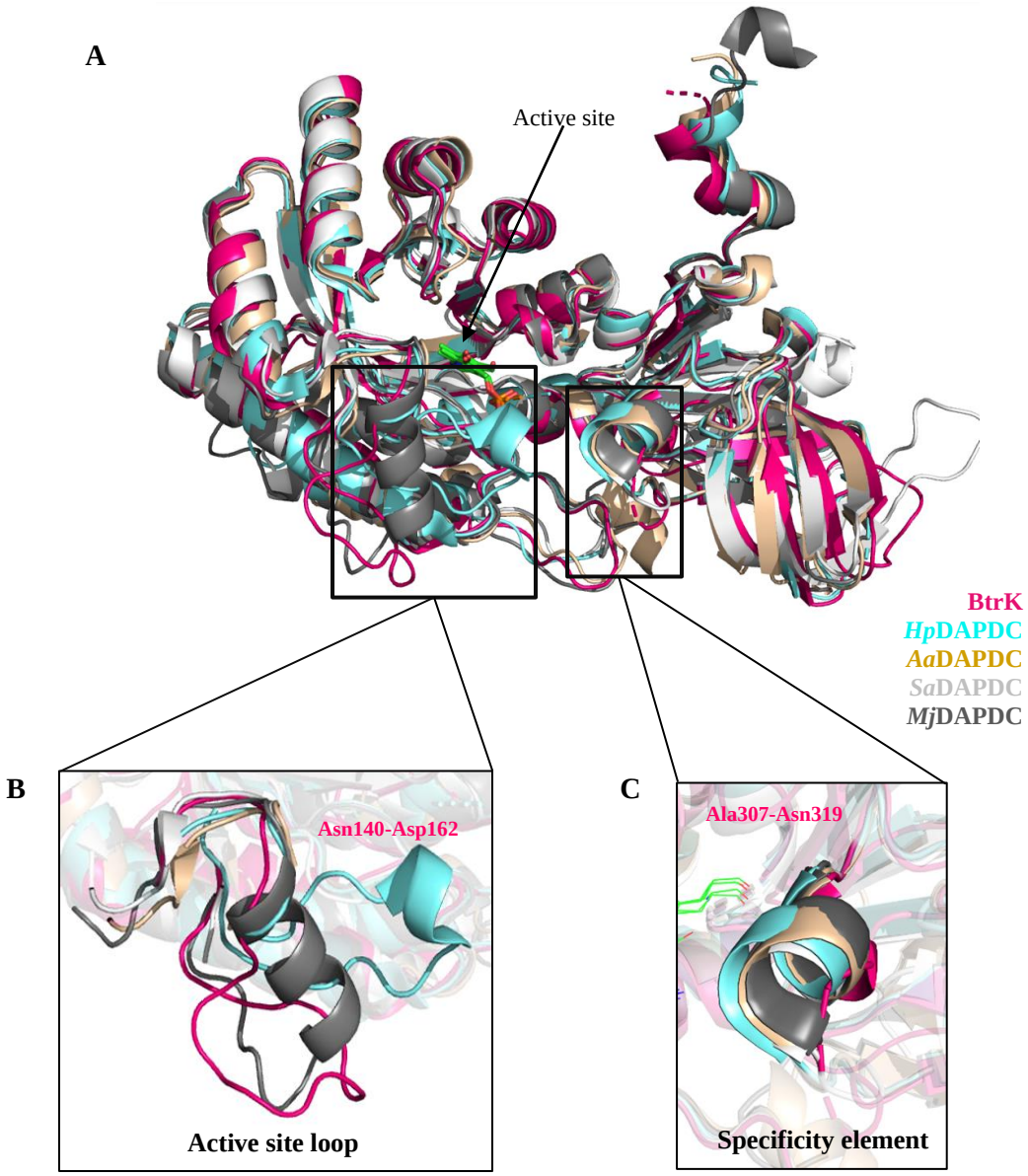

Fig. 3. (A) Superposition of BtrK and the closest DAPDC homologs. BtrK (PDB 7ru7) is in pink; *Hp*DAPDC (PDB 2qgh) is in cyan; *Aa*DAPDC (PDB 2p3e) is in wheat; *Sa*DAPDC (PDB 6kni) is in white; and *Mj*DAPDC (PDB 1twi) is in grey. (B) A closer view of the active site loop superposition. (C) A closer view of the specificity element superposition.

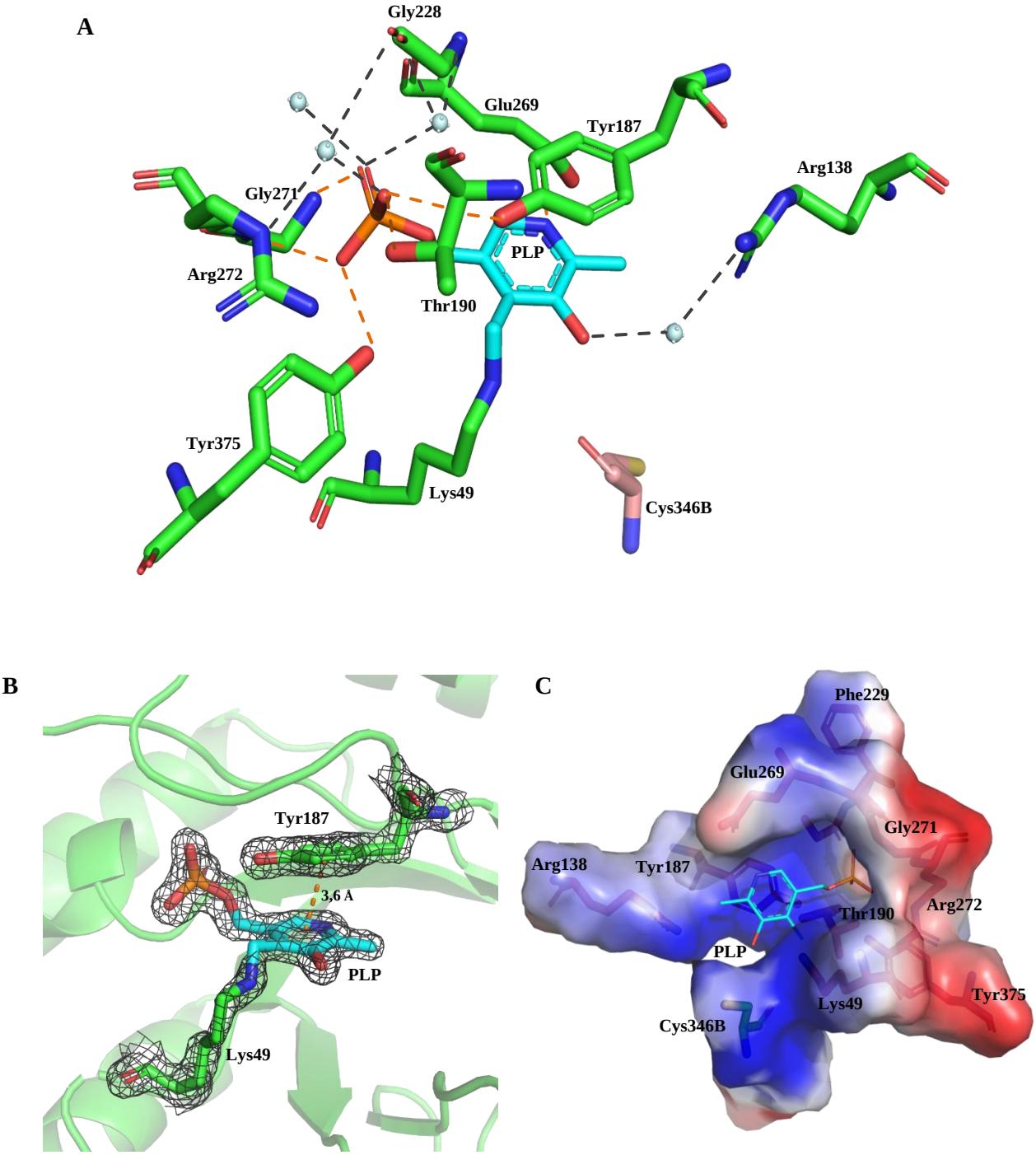

Fig. 4. The active site of BtrK. (A) Stick representation of the PLP (cyan) and the closest amino acids. Carbons of residues from chain A are colored in green and the Cys346 from the adjacent chain is identified in pink. Waters are shown as light blue spheres. Direct atomic interactions and via water molecules are represented in orange and grey dashed lines, respectively. (B) Electron density trace (2Fo-Fc map) of the covalent ligation between PLP and Lys49, and the π-stacking with the Tyr187. (C) The electrostatic potential surface of the PLP binding site. Electronegative and electropositive regions are in red and blue, respectively.

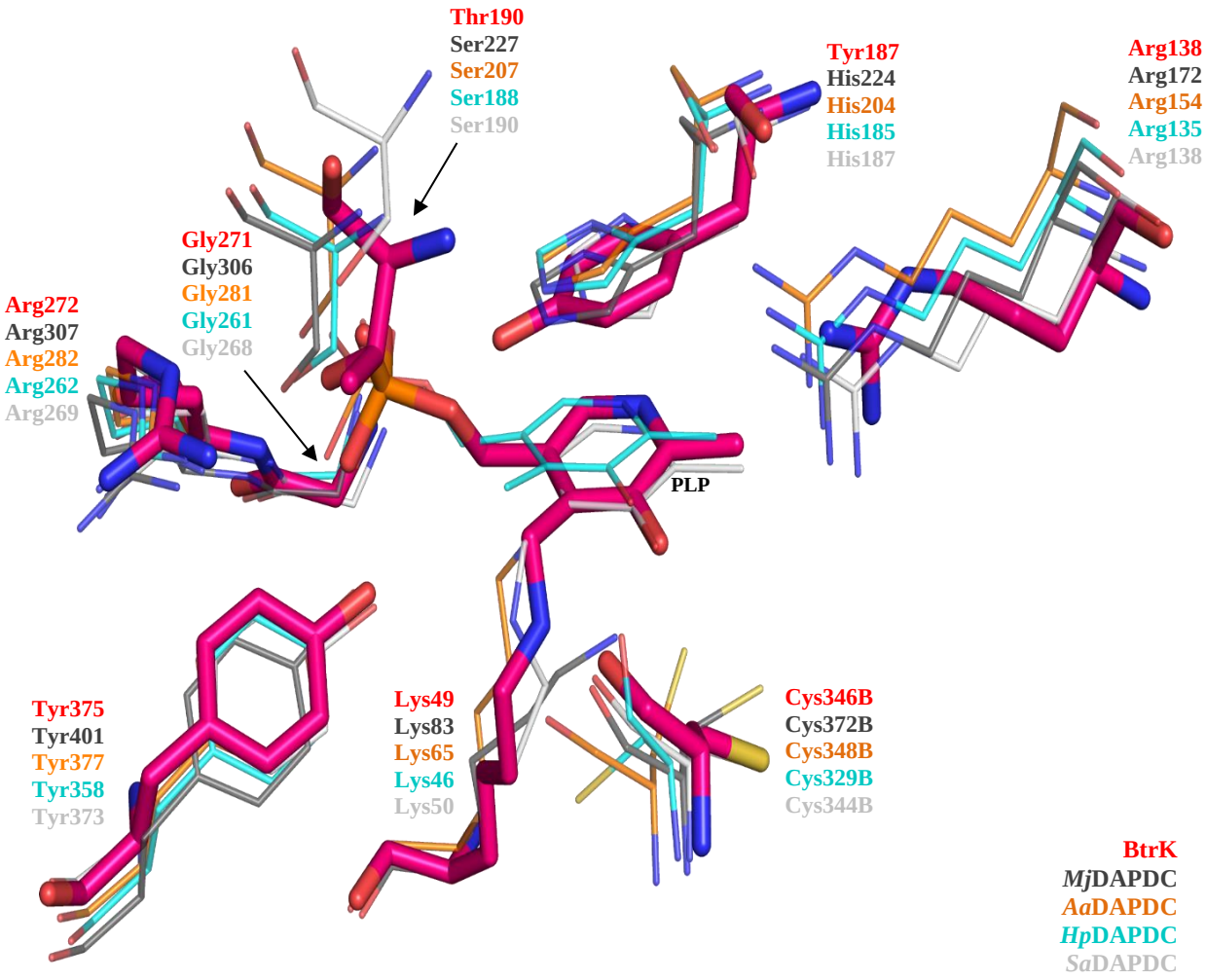

Fig. 5. Superposition of BtrK active site and the different DAPDC. BtrK residues are represented in stick and the residues from other DAPDC are shown as lines. The carbons in pink are from BtrK; in grey from *Mj*DAPDC; in orange from *Aa*DAPDC; in cyan from *Hp*DAPDC and in white from *Sa*DAPDC.

A

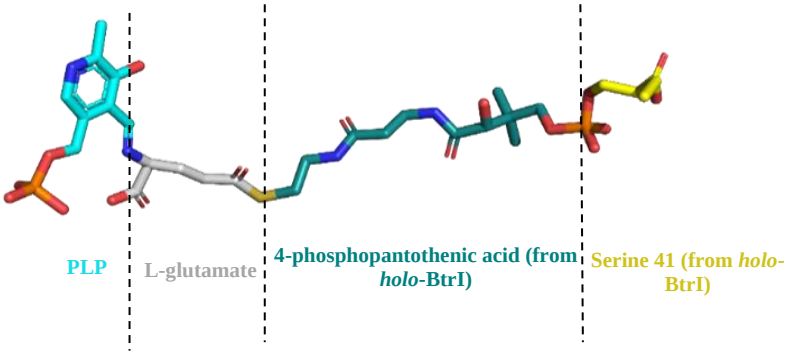
PLP
L-glutamate
4-phosphopantothenic acid (from *holo*-BtrI)
Serine 41 (from *holo*-BtrI)

B

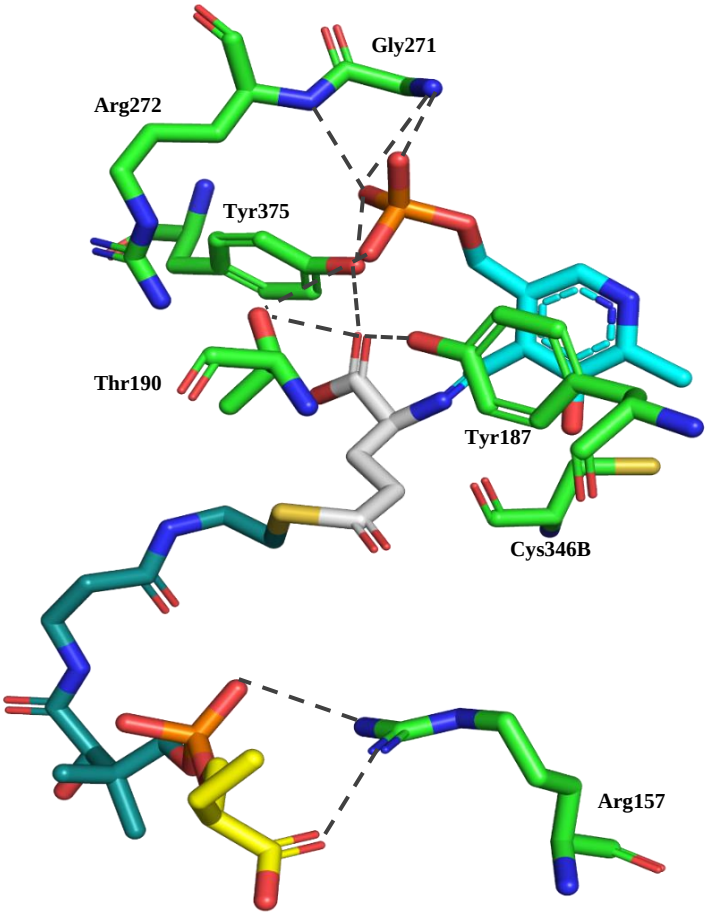
Gly271
Arg272
Tyr375
Thr190
Tyr187
Cys346B
Arg157

C

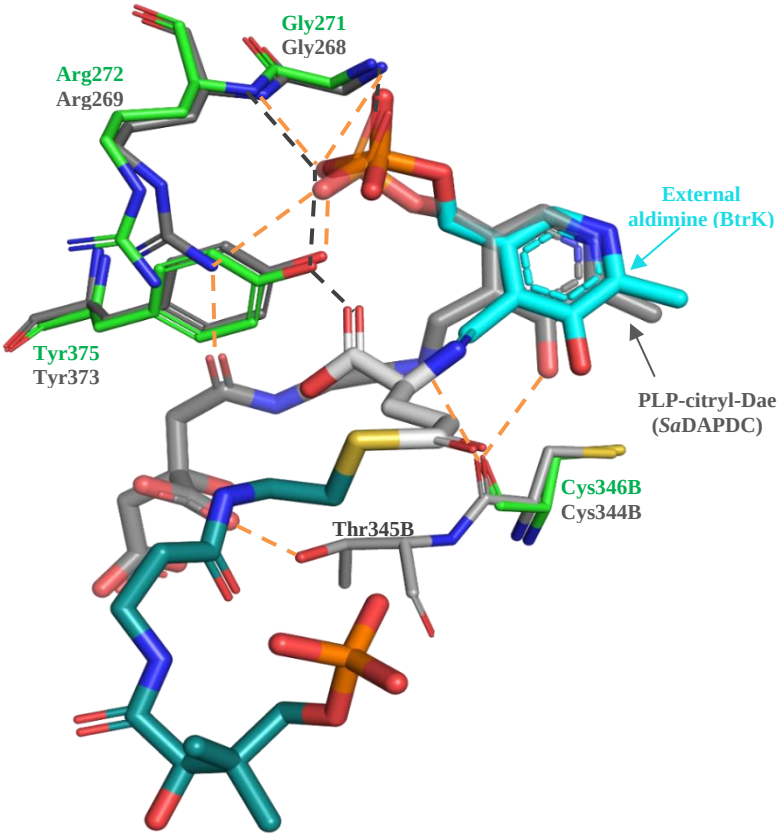
Gly271
Gly268
Arg272
Arg269
External
aldimine (BtrK)
Tyr375
Tyr373
PLP-citryl-Dae
(*Sa*DAPDC)
Cys346B
Cys344B
Thr345B

D

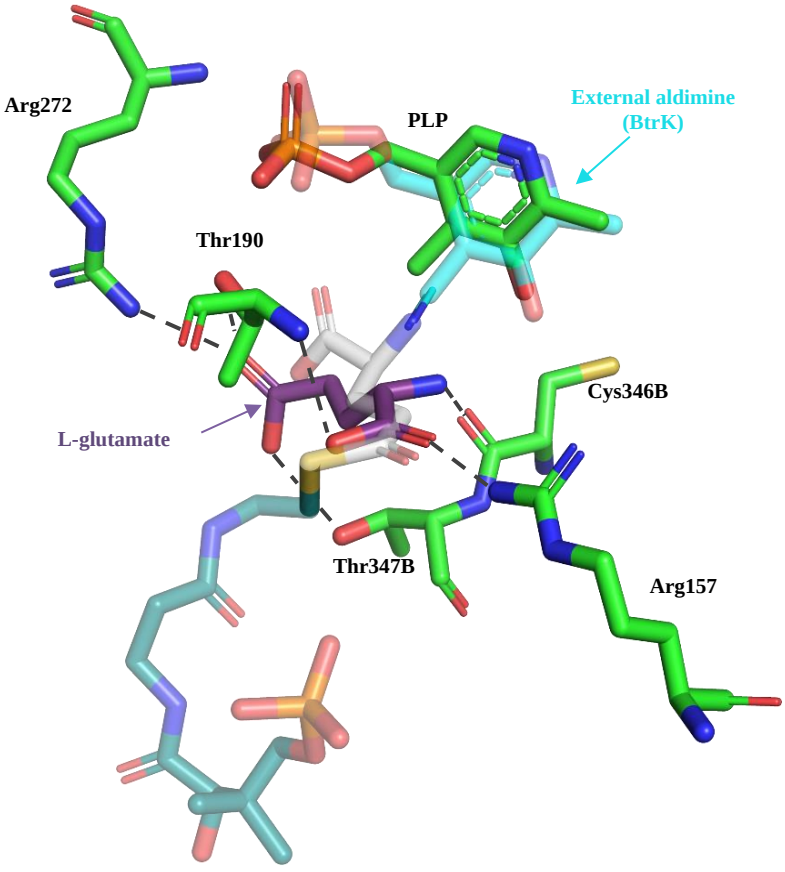
Arg272
PLP
External aldimine
(BtrK)
Thr190
Cys346B
L-glutamate
Thr347B
Arg157

Fig. 6. Docking of PLP-*O*-[*S*-γ-Lglutaylpantetheine-4'-phosphate]serine and L-glutamate into BtrK active site. (A) Representation of the truncated substrate or external aldimine identified by different colors. (B) Possible external aldimine formation of the BtrK decarboxylation reaction. Colors are according to A. Polar bonds are represented in dark dashed lines. (C) Superposition of the BtrK and *Sa*DAPDC structures and their respective substrates. BtrK and *Sa*DAPDC residues are in green and grey sticks, respectively. The PLP-citryl-Dae of the *Sa*DAPDC is in grey sticks. Polar bonds between the BtrK and its substrate are in dark dashed lines; between *Sa*DAPDC and its substrate are in orange dashed lines. (D) Possible interaction between L-glutamate and BtrK. External aldimine is also shown in sticks with a certain degree of transparency to compare the position. Polar bonds are represented in dark dashed lines.

Table 1 Data collection and processing for BtrK-PLP

Diffraction source	PETRA III -Desy/Germany
Wavelength (Å)	0.976260
Temperature (K)	100
Detector	Pilatus 6M
Crystal-detector distance (mm)	243.6
Rotation range per image (°)	0.2
Total rotation range (°)	360
Exposure time per image (s)	0.1
Space group	P 21 21 2
a, *b*, *c* (Å)	71.9, 129.5, 45.7
α, β, γ (°)	90 90 90
Resolution range (Å)	43.11-1.4 0(1.45-1.40)
Total No. of reflections	1104231 (108595)
No. of unique reflections	84760 (8305)
Completeness (%)	99.89 (99.38)
Redundancy	13.0 (13.1)
$\langle I/\sigma(I)\rangle$	21.21 (1.01)
$R_{\text{r.i.m.}}$	0.01614 (0.5621)
CC1/2	1 (0.617)
Overall *B* factor from Wilson plot (Å^2)	22.18

Values for the outer shell are given in parentheses.

Table 2 Structure solution and refinement for BtrK-PLP

PDB entry	7RU7
Resolution range (Å)	43.11 - 1.40 (1.45 - 1.40)
Completeness (%)	99.89 (99.38)
No. of reflections, working set	84753 (8305)
No. of reflections, test set	4190 (407)
Final R_{cryst}	0.178 (0.308)
Final R_{free}	0.195 (0.329)
No. of non-H atoms	
Protein	3648
Ligand	22
Water	343
Total	3648
R.m.s. deviations	
Bonds (Å)	0.007
Angles (°)	1.15
Average *B* factors (Å^2)	30.94
Protein	30.08
Ligand	28.85
Water	39.27
Ramachandran plot	
Most favored (%)	96.29
Allowed (%)	3.47
outliers	0.25

Values for the outer shell are given in parentheses.